Engineering and Laboratory Note

applied optics

Digital lensless holographic microscopy: numerical simulation and reconstruction with ImageJ

Carlos Trujillo,[1,*] Pablo Piedrahita-Quintero,[2] and Jorge Garcia-Sucerquia[2]

[1]Applied Optics Group, Physical Sciences Department, School of Science, Universidad EAFIT, Medellín, Colombia
[2]School of Physics, Universidad Nacional de Colombia—Sede Medellin, A.A: 3840, Medellin 050034, Colombia
*Corresponding author: catrujilla@eafit.edu.co

Received 23 April 2020; revised 25 May 2020; accepted 28 May 2020; posted 28 May 2020 (Doc. ID 395672); published 30 June 2020

The description and validation of an ImageJ open-source plugin to numerically simulate and reconstruct digital lensless holographic microscopy (DLHM) holograms are presented. Two modules compose the presented plugin: the simulation module implements a discrete version of the Rayleigh–Somerfield diffraction formula, which allows the user to directly build a simulated hologram from a known phase and/or amplitude object by just introducing the geometry parameters of the simulated setup; the plugin's reconstruction module implements a discrete version of the Kirchhoff–Helmholtz diffraction integral, thus allowing the user to reconstruct DLHM holograms by introducing the parameters of the acquisition setup and the desired reconstruction distance. The plugin offers the two said modules within the robust environment provided by a complete set of built-in tools for image processing available in ImageJ. While the simulation module has been validated through the evaluation of the forecasted lateral resolution of a DLHM setup in terms of the numerical aperture, the reconstruction module is tested by means of reconstructing experimental DLHM holograms of biological samples.

https://doi.org/10.1364/AO.395672

1. INTRODUCTION AND FUNDAMENTALS

Digital lensless holographic microscopy (DLHM) is perhaps the simplest architecture of state-of-the-art of microscopy techniques. Understood as a modern realization of Gabor's invention of holography [1] with the use of digital cameras and computers, DLHM is also a two-stage imaging method. A point source and digital camera are the needed hardware in the recording stage, and a specific numerical wave propagation algorithm is necessary in the reconstruction process [2]. The said simplicity, the capability of micrometer-sized lateral resolution [3,4], its portability [5], and its intrinsic possibility of being cost-effective [6] has spread the use of DLHM in applications in life [7–9] and material sciences [10,11]. The state-of-the-art of DLHM features the said cost-effective way of building and promises further field portability [12], which will widen its spectrum of applications. As a contribution to help the easy use this powerful microscopy technology, in this work it is introduced as an ImageJ [13] plugin that embraces a simulation and a reconstruction module for DLHM. The idea of embedding the DLHM plugin in ImageJ resorts to (i) the possibility of the direct use of the hundreds of image processing tools that are already built into the said program and (ii) the open-source philosophy of this project. The simulation module is aimed to provide an easy way to produce DLHM holograms for amplitude and/or phase objects modeled via 2D gray-level images. The simulated holograms or those recorded in a real DLHM setup can be reconstructed in a reconstruction module, which provides a user-friendly interface to make, for instance, step-by-step or batch reconstructions. For both modules, the built-in tools of ImageJ are available to the user in the simulation module, for example, to create any thought amplitude and/or phase object and produce the corresponding DLHM hologram and, in the reconstruction module, for instance, to produce videos of stacked reconstruction planes. In the following paragraphs, the physics fundamentals underlying the developed plugin are presented without the aim of making this work fully self-contained. Readers interested in the numerical details of the plugin implementation are referred to the appropriate literature.

A. Simulation Module

To simulate a DLHM hologram, one can consider that, in the recording stage, the sample transmittance $S(\vec{r}_0)$, placed at a distance z from the point source, is illuminated by a diverging spherical wavefront $\exp[ik\vec{r}]/|\vec{r}|$. The diffracted wavefield is magnified by free-space propagation to reach a digital camera, L, apart from the point source. In this description, the recording stage can be modeled with the help of the position vectors measured from the point source $\vec{r}_0 = (x_0, y_0, z)$ and $\vec{r} = (x, y, L)$ to denote the sample plane and the digital camera

plane, respectively. The complex-valued diffracted wavefield reaching the plane of the digital camera can be therefore described by means of the Rayleigh–Somerfield diffraction formula [14]:

$$U(\vec{r}) = \int_{\text{Sample}} S(\vec{r}_0)\, \frac{\exp\left[ik\vec{r}_0\right]}{|\vec{r}_0|}\, \frac{\exp\left[ik\,(\vec{r}-\vec{r}_0)\right]}{|\vec{r}-\vec{r}_0|}\, \mathrm{d}\vec{r}_0. \quad \textbf{(1)}$$

The free-space magnification of the diffraction pattern in Eq. (1) is determined by the ratio $M = L/z$. This value of M has to be chosen such that (i) the diffraction pattern is correctly sampled by the digital camera and (ii) the magnified region of interest of the sample fits in the digital camera. These two geometrical conditions, along with the fact of using weak scattering samples [1], have to be considered for DLHM to work properly. The recording stage produces the intensity distribution recorded at the digital camera plane:

$$I(\vec{r}) = U(\vec{r})\, U^*(\vec{r}), \quad \textbf{(2)}$$

with $*$ denoting the complex conjugate. This intensity distribution, known as the in-line hologram [2], constitutes the main output of the simulation module and input from which the sample information can be retrieved in the reconstruction stage.

B. Reconstruction Module

Following the principles of holography [1,15], the information of the sample $S(\vec{r}_0)$ is reconstructed in DLHM by evaluating the diffraction process that a converging spherical wavefront $\exp[-ik\vec{r}]/|\vec{r}|$ undergoes as it illuminates the in-line hologram $I(\vec{r})$ and propagates toward the sample plane. The practical implementation of the reconstruction in DLHM uses a contrast hologram $\tilde{I}(\vec{r})$ instead of the direct recorded in-line hologram; further, $\tilde{I}(\vec{r})$ can be a pixel-wise subtraction between $I(\vec{r})$ and the recorded intensity with no sample present. As in DLHM, the in-line hologram or, in general, the contrast hologram is a digital image produced in the simulation module or recorded in a real DLHM setup. This diffraction process can be numerically described by means of a scalar diffraction formula [14]:

$$S(\vec{r}_0) = \int_{\text{Digital Screen}} \tilde{I}(\vec{r})\, \frac{\exp\left[-ik\vec{r}\right]}{|\vec{r}|}\, \frac{\exp\left[-ik\,(\vec{r}-\vec{r}_0)\right]}{|\vec{r}-\vec{r}_0|}\, \mathrm{d}\vec{r}. \quad \textbf{(3)}$$

The result of Eq. (3) is a complex-valued quantity from which one can compute its intensity $S(\vec{r}_0)S^*(\vec{r}_0)$ or phase $\phi(\vec{r}_0) = \arctan(\mathrm{Im}[S(\vec{r}_0)]/\mathrm{Re}[S(\vec{r}_0)])$, with Im and Re the imaginary and real parts, respectively. The evaluation of this diffraction process in different planes of propagation starting from the digital camera to the point source allows the production of a stack of reconstructed images that could be utilized to produce a 3D recreation of the sample, within the restriction of axial resolution of DLHM [2].

Analytically, Eqs. (1) and (3) are the mathematical support to simulate and reconstruct DLHM holograms, in that order. However, both numerical implementations in the presented plugin impose the fulfilling of the sampling theorem [14] and embracing the two-folded daunting features of allowing pixel resizing at will with the propagation and being applicable for high numerical apertures (NA), i.e., NA > 0.2. For the simulation module, these features are reached via the Fresnel–Bluestien transform [16], along with fulfilling the geometrical constrains that guarantee the accomplish of the sampling theorem and a coordinate remapping to interpolate the evenly simulated in-line hologram. Readers interested in the details of the numerical implementation of Eq. (1) done in the present plugin are referred to [17]. For the numerical implementation of Eq. (3) in the reconstruction module, once again the main challenges involve the realization of an algorithm that allows pixel resizing at will, as the numerical wavefront propagates from the digital camera plane toward the point source and the applicability of the said algorithm to high NAs. With the last requirement in mind, one could be tempted to use the angular spectrum method [18–20]. However, because the angular spectrum is essentially a convolution approach, it does not allow us directly to change the pixel size at will as the wavefront propagates. A coordinates transformation [11,12], inspired in the seminal Kreuzer's work [21], and the use of the Fresnel–Bluestein transform [16], turn the propagation integral in Eq. (3) into a circular convolution to enable its computation via fast Fourier transforms (FFT) [22], pixel size controlled at will and applicable to high NAs. The state of the art of the implementation of the said reconstruction algorithm uses a graphics processing unit (GPU) to reconstruct DLHM holograms at video rates [23]; this GPU implementation is also available when the present plugin is run in a computer powered with a GPU. As the aim of this work is to introduce the ImageJ plugin of the two modules to simulate and reconstruct DLHM holograms, we refer readers interested in the details of the numerical implementation of each module to the corresponding literature; for the case of the reconstruction plugin, details of the implementation of the reconstruction module can be read elsewhere [24,25].

2. DLHM PLUGIN

A. Plugin Installation

To install the DLHM plugin, the following steps must be executed:

i) Download and install the latest ImageJ version as instructed in [26].
ii) Download all the required libraries available in the Downloads section in [27]. These libraries are DLHM.jar, JTransforms.jar [28], and JDiffration.jar [23]; these libraries are also zipped into the file DLHM_1.1-libs.rar or in the file DLHM_1.1.jar, which can be downloaded in the Download section in [27]. After downloading, extract its content in the folder imagej/plugins.
iii) A folder named OD, which includes the latter three libraries, must be copied into the imagej/plugins folder.
iv) For the completeness of available tools to work along with the DLHM plugin, the "Numerical Propagation" plugin [29] should also be installed. The installation procedure is the same as for the DLHM plugin: download all the required libraries by clicking over NumericalPropagation_1.2.jar or NumericalPropagation_1.2-libs.zip link in the Download section of [29] then extract its contents in the imagej/plugins folder as well.

Fig. 1. ImageJ graphical user interface. See the OD menu, under which the DLHM is located.

B. DLHM Plugin Main Features

Once the DLHM plugin has been properly installed, it can be accessed in the ImageJ graphical user interface (GUI) via OD/DLHM menus, as shown in Fig. 1. Three options are available: Simulation, Reconstruction, and About DLHM. The first two options allow us to initiate the numerical simulation and reconstruction modules. The About DLHM option displays an information window with details of the opto-digital processing group and the plugin itself. In the same way, the OD menu includes, if installed, the Numerical Propagation plugin [20], also developed within our research group.

Taking advantage of the feature of ImageJ that eases the operation with images, the DLHM plugin utilizes file images as the data containing the amplitude and phase components needed in the two modules of the plugin; one image must be provided to represent either the amplitude or the phase or for both. Once, at least one image is loaded into the ImageJ environment, the two modules of the plugin can access to them to use in the simulation or reconstruction process. Although the details of each of the components of the DLHM plugin and their use can be read in its documentation [27], here we present a brief summary of its operation for a quick reference.

1. DLHM Simulation Module

When the DLHM simulation module is called, a GUI pops up. This GUI is composed of four panels: (1) Parameters, (2) Log, (3) Outputs, and (4) Buttons, as shown in Fig. 2. In the panel Parameters of this GUI, the gray-level images that represent the Amplitude and Phase and the geometrical parameters of the simulated DLHM setup are inserted; these parameters include Wavelength, the source-to-sample, So.–Sa. dist. and source-to-screen So.–Sc. distances, and the Screen width and Screen height. The Manual and Automatic radio buttons determine whether the sample window dimensions are fixed by the user manually or calculated by the plugin automatically using the geometry of the DLHM setup. In the log panel, the recent history of the plugin usage is displayed; this history consists of the selected parameters in every launched DLHM simulation. The outputs panel provides different options for the outcome of the simulation. Hologram considers the modelling of the DLHM in-line hologram as described by Eq. (2) with the sample present; Reference is the resulting intensity of the numerical propagation with no sample present; Contrast hologram is built by pixel-wise subtracting the Hologram and Reference outputs. The simulation can be launched in the panel buttons. In the same panel, the units of the geometrical parameters of the modeled DLHM setup can be customized using the Settings button.

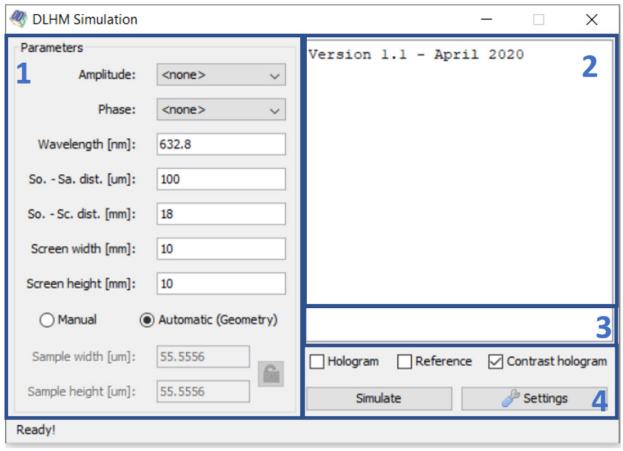

Fig. 2. DLHM simulation module main window. See text for further details.

2 DLHM Reconstruction Module

The GUI related to the reconstruction is also composed of four panels: (1) Parameters, (2) Log, (3) Outputs, and (4) Buttons, as shown in Fig. 3. The Parameters (1) panel allows the user to select the Hologram to be reconstructed, the Reference to compute the contrast hologram, i.e., an optional hologram with no sample present, the illumination wavelength, and the geometrical parameters of the DLHM setup, i.e., Reconst. dist. the source-to-sample distance, and So.–Sc. dist. the source-to-screen distance. Input width and Input height set the physical dimensions of the input images, Hologram and Reference. In this panel, there are also two options to set the physical size of the output image; Manual allows the user to manually determine the size of the reconstructed hologram in the Output width and Output height boxes; the Automatic (Geometry) radio button selects an automatically calculation of this size by using triangle relations with the illumination cone and the source-to-sample distance. In the log (2) panel, the recent history of the plugin usage is displayed; this history consists of the selected parameters in every launched reconstruction. In the outputs (3) panel, different options to visualize the output of the reconstructed wavefield are provided, including Phase, Amplitude,

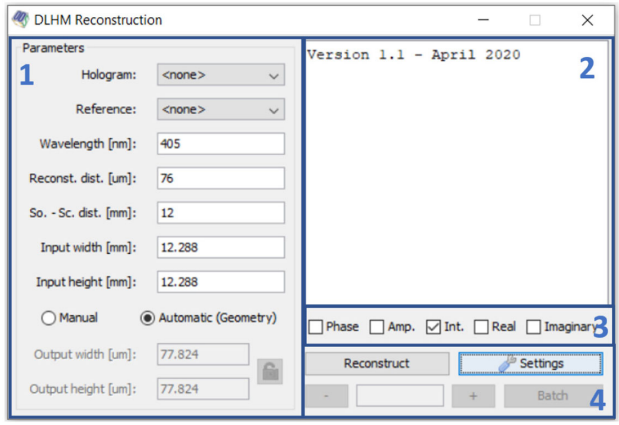

Fig. 3. DLHM reconstruction module main window. See text for further details.

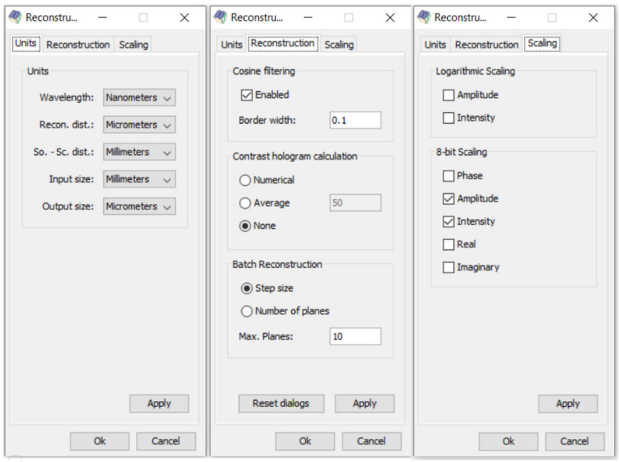

Fig. 4. Customization window tabs of the DLHM reconstruction module. See text for further details.

Intensity, and the production of the Real and Imaginary components of the complex-valued reconstructed wavefield. The lower right (4) panel of the reconstruction module includes three buttons that allow (i) to Reconstruct a DLHM hologram according to the Parameters panel, (ii) to customize different Settings for the numerical reconstruction, shown in Fig. 4, and (iii) to launch the Batch mode. Options that can be customized in the settings window include the possibility to change the Units of the geometrical parameters, a set of options for the Reconstruction as to whether Cosine filtering is applied before the reconstruction, the Contrast hologram calculation method, the Batch Reconstruction, and the Scaling of the image representations, which can be useful for post-processing purposes of the images. The Contrast hologram calculation method and the Batch Reconstruction are two special features of the plugin that deserve further description.

As for the Contrast hologram calculation method, the plugin considers two options. First, if a reference image is previously loaded, the contrast hologram is the pixel-wise subtraction between the hologram and the reference images. The second option arises when no reference image is loaded; in this case, there are three different options to build the contrast hologram: (i) A Numerical option in which the pixel-wise subtraction of the hologram and a modeled spherical wave whose radius of curvature is the distance from the point source to the screen is the contrast hologram; (ii) An Average option in which the pixel-wise subtraction between the hologram and average values, calculated for different regions of the hologram, compose the contrast hologram; these regions are squares whose side size is determined by the user in the text box related to this option; (iii) a None option in which the contrast hologram is the hologram loaded in the parameters with no modifications at all.

The Batch reconstruction mode available in the DLHM plugin is accessible via the Batch button present in the reconstruction window. Batch reconstruction consists in a bundle of reconstructed images produced by a sweep of the reconstruction distance. The hologram is numerically reconstructed using all the selected parameters in the Parameters panel with the exception of the source-to-sample distance and the output width/height. The Reconst. dist., the source-to-sample distances are determined by inserting the starting and ending source-to-sample distances and the number of planes or the step distance between reconstruction planes. The Output width and Output height for the resulting reconstructions are given by the selected parameters when the Batch button is clicked; this option produces all the resulting reconstructions with the same output width/height. Otherwise, an Automatic option can be selected to calculate the new output dimensions using the geometry relations for each reconstruction plane.

One of the key features of the development of the simulation and/or the reconstruction modules of the DLHM plugin within the ImageJ environment is the possibility of direct use of the whole set of built-in tools for image processing that ImageJ provides in an open source philosophy; within this environment, the user can manipulate and analyze the resulting output images by means of histograms, brightness adjusting, contrast measurements, specimen counting, and three-dimensional plotting, among the many other useful opportunities that are immediately available in ImageJ.

3. NUMERICAL SIMULATIONS OF DLHM HOLOGRAMS

To illustrate the use of the simulation module of DLHM, initially, a hologram of a gray-level image sample of a diatom microalgae is modeled. The input image to simulate this hologram is presented in Fig. 5, Panel (a). This image was acquired in a phase contrast microscope employing LED illumination, a CCD camera of 1024 × 0124 square pixels, and a 40× microscope objective with 0.65 numerical aperture. The modeled hologram emulates a recorded hologram with a sensor camera of 1024 × 1024 square pixels of 6 μm for each side; the sample is numerically illuminated by a 405 nm point source located at 10 mm from the center of the camera. The hologram was built with the sample placed 300 μm from the point source. In the simulation module of the plugin, the input image was selected to be an amplitude input only. The geometrical parameteres of the modeled DLHM setup were input as previously described, including automatic determination of the sample width/height in order to simulate a sample of approximately 45 μm in diameter, which is within the typical size of a diatom according to the literature [30]. The resulting hologram and reference images for this sample are presented in Panels (b) and (c) of Fig. 5, respectively. To validate the latter results, both resulting images were input in the reconstruction module. By entering the same parameters of the DLHM geometry used to model the hologram, except for the source-to-sample distance, which, after a batch reconstruction, was determined to be 305 μm, an intensity reconstruction was obtained [see Panel (d) of Fig. 5]. As can be seen in the intensity reconstruction of this simulated hologram, most of the details of the original sample image are properly reconstructed except for some noise surrounding the specimen, which is due to the diffraction-associated phenomena underlying the DLHM. The input amplitude image, hologram, reference, and reconstruction for this DLHM simulation are available via direct download in the *Examples* section of [27].

As a second illustration of the use of the simulation module of DLHM, the relationship between the lateral resolution of

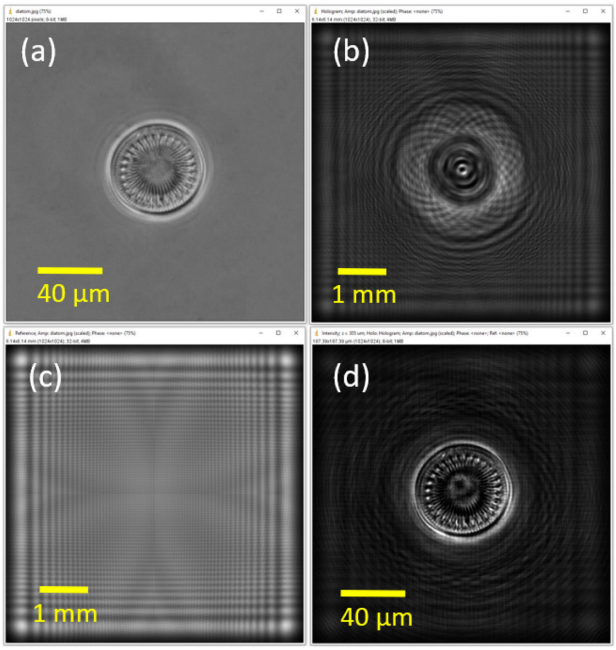

Fig. 5. DLHM simulation of a diatom microalgae sample. (a) Phase-contrast image used as an amplitude input to the simulation module. (b) Simulated DLHM hologram. (c) Simulated reference DLHM hologram. (d) Intensity reconstruction of the subtraction of the simulated hologram and the simulated reference hologram.

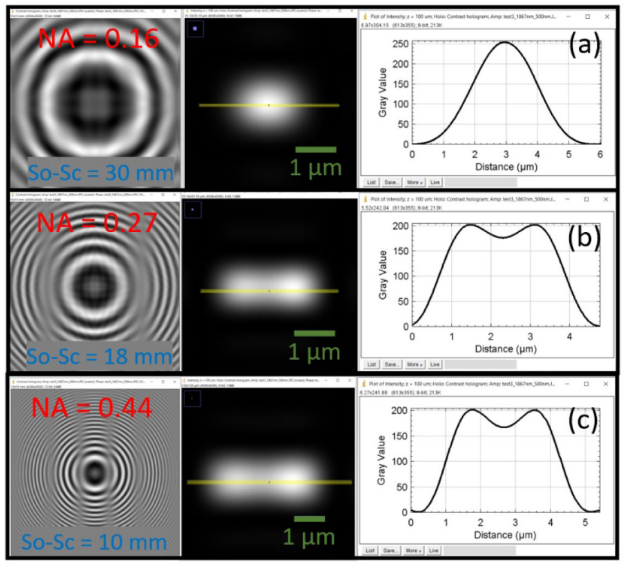

Fig. 6. Simulation of DLHM holograms (left) and their intensity reconstructions (center) for a sample with a separation $S = 1.9$ µm between circular stops. For the yellow line in the intensity reconstruction, a profile line has been plotted (right). DLHM setups of (a) 0.16 NA Panel, (b) 0.27 NA Panel, and (c) 0.44 NA Panel have been modeled.

DLHM and its numerical aperture is revisited; to this aim, holograms of circular stops as samples were simulated and then reconstructed with the reconstruction module. The results were analyzed with the Line Profile built-in tool of ImageJ. In DLHM, two point objects illuminated with a wavelength λ are perfectly distinguished if the distance between them S fulfils the condition [2]

$$S \geq \frac{\lambda}{2\mathrm{NA}}. \tag{4}$$

As no lenses are used for the recording of the diffracted wavefield, the NAis given by the simple geometry of the DLHM setup, upon the mandatory condition that the full width of the digital sensor W is completely illuminated:

$$\mathrm{NA} = \frac{W}{2\sqrt{\left(\frac{W}{2}\right)^2 + L^2}}. \tag{5}$$

In Eq. (5), W is width of the digital screen and L is the source-to-screen distance. To numerically validate Eq. (4), DLHM holograms using as amplitude input two circular stops of 500 nm in diameter with a separation between their centers of $S = 1.9$ µm in a white screen, are created. The sample plane was numerically located at 100 µm from the point source and its width and height are manually fixed to be 50 µm, regardless of the source-to-screen distance, i.e., regardless of the numerical aperture of the setup. A monochromatic point source of 632.8 nm was simulated to illuminate a 10 mm × 10 mm digital screen of 4096 × 4096 square pixels; hence, the amplitude input images are composed of 4096 × 4096 square pixels as well. For this sample, three holograms were simulated with source-to-screen distances of 30, 18, and 10 mm. Since the simulated digital screen dimensions are 10 mm × 10 mm, then, by using Eq. (5), the said source-to-screen distances yield to NAs of 0.16, 0.27, and 0.44, respectively. For each one of these numerical apertures, three outputs are obtained: (i) the simulated DLHM hologram, left-hand-side column of Fig. 6; (ii) a zoomed-in DLHM intensity reconstruction, center column of Fig. 6; and (iii) a profile line, right-hand-side column of Fig. 6. The results for the setup of NA = 0.16 in Panel (a) show that the two stops are not resolved, which is expected for a lateral resolution of 1978 nm according with Eq. (4). Conversely, in the results for setup of NA = 0.27 Panel (b) and NA = 0.44 Panel (c), the stops are resolved [31] as expected for theoretical lateral resolutions of 1217 and 719 nm, in that order. Additionally, using the built-in Line Profile tool of ImageJ, a separation of 1.9 µm between the two reconstructed objects is measured via the two peaks of the curves in the profile lines on the right of these two panels. The input amplitude image, constrast holograms, and intensity reconstructions for this study are all available via direct download in the Examples section in [27].

The above results validate the use of the simulation module of the developed plugin in tasks involving the modelling of DLHM holograms. These tasks can be addressed either by employing experimental image samples obtained via other microscopic setups or by numerically modelling the input samples to test different features of DLHM. All the latter within the robust environment of ImageJ.

4. NUMERICAL RECONSTRUCTIONS OF DLHM HOLOGRAMS

In this section, the numerical reconstruction of experimental DLHM holograms by using the developed plugin is presented.

Initially, an experimental hologram of a microorganism is acquired. This hologram was recorded in a DLHM setup with a source-to-screen distance of 11 mm, employing a 532 nm wavelength laser and a CCD camera of 2048 × 2048 square pixels, whose side size is 6 μm, i.e., a 12.288 mm input height/width. A rough reconstruction estimates an in-focus image of the sample somewhere between 870 to 950 μm from the point source. By entering the latter parameters in the reconstruction module of the plugin, and using as inputs the hologram, Fig. 7 Panel (a), and the reference hologram in Panel (b) of the same figure, reconstructions both in amplitude, Panel (c), and in intensity, Panel (d) of Fig. 7, are immediately obtained after pressing the Reconstruct button.

As can be observed in the zoomed-in areas encircled by red lines both in the amplitude and intensity reconstructions of Fig. 7, to establish whether or not the object is in focus, is a nontrivial task. The latter considering the 938 μm × 938 μm field of view automatically calculated by the plugin according to the source-to-sample distance. To improve the visualization of the specimen, the output width and height have been manually fixed to 100 μm. By including this change and the same reconstruction parameters employed for the reconstructions in Fig. 7, a batch reconstruction of the hologram from 870 to 950 μm, with a step reconstruction distance of 10 μm, has been launched; the resulting intensity images can be observed in Fig. 8. By moving the horizontal sliding bar provided in the output stack of this batch reconstruction, it is visually determined that the specimen is in-focus at a source-to-sample distance of 910 μm, as can be checked in Panel (e) of Fig. 8.

For a second experimental validation, a hologram containing the information of four microorganisms has been selected to be processed by the developed plugin. This DLHM hologram was recorded with the same laser as the illuminating source

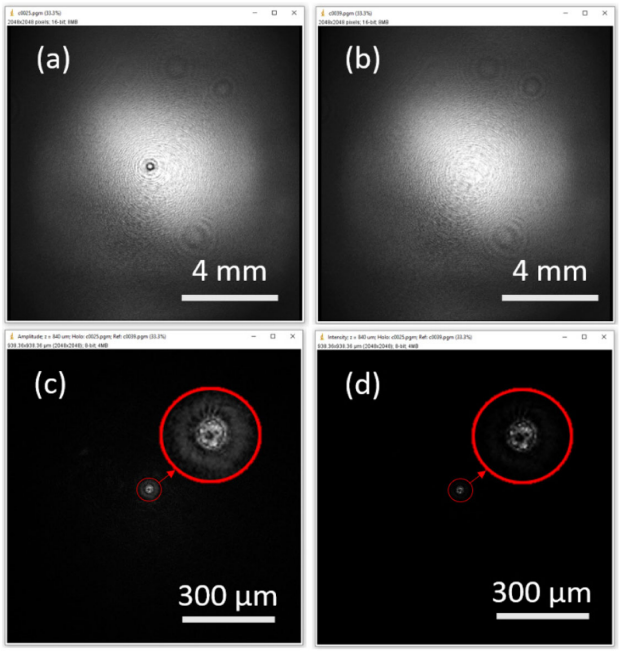

Fig. 7. DLHM reconstruction of an experimental hologram of a microorganism. (a) DLHM hologram with sample. (b) DLHM hologram with no sample. (c) Amplitude DLHM reconstruction. (d) Intensity DLHM reconstruction.

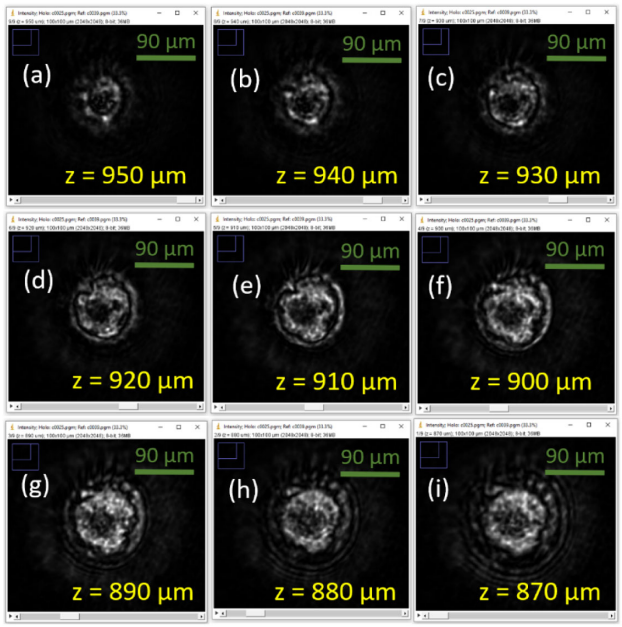

Fig. 8. Intensity reconstructions using the batch mode of the DLHM plugin. From (a) to (i), the source-to-sample distance is decreased from 950 to 840 μm with a 10 μm step.

and the same CCD camera to that of Fig. 7. For this hologram, the source-to-screen distance was 9 mm and the specimens are expected to be located somewhere between 400 to 600 μm from the point source. By using the latter parameters and fixing the output width and height to 470 μm, a batch reconstruction has been launched with a reconstruction distance step of 1 μm. In Fig. 9, four particular reconstructed planes are displayed; in each of these planes, a different microorganism is in focus (red circle), while the other three are out of focus (blue circle), as

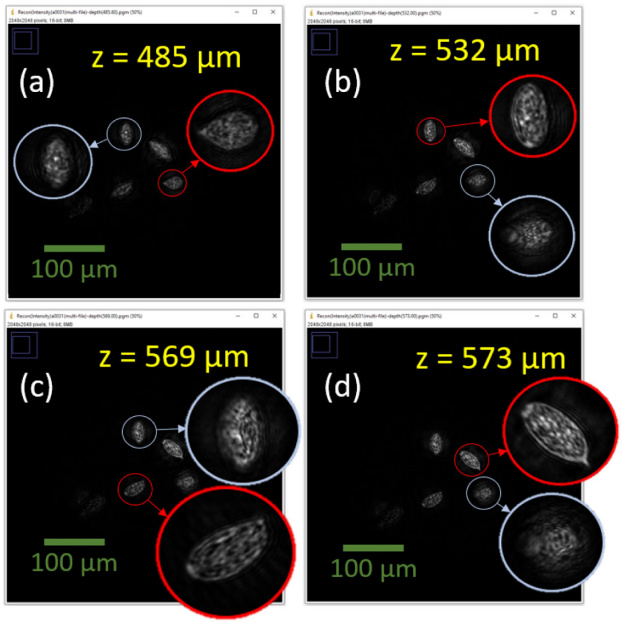

Fig. 9. Intensity DLHM reconstructions for different source-to-sample distances in which each one of the four microorganisms is properly focused.

shown in the zoomed-in areas. Therefore, by using the DLHM reconstruction module, the process to manually focus different specimens from a single DLHM hologram is considerably eased.

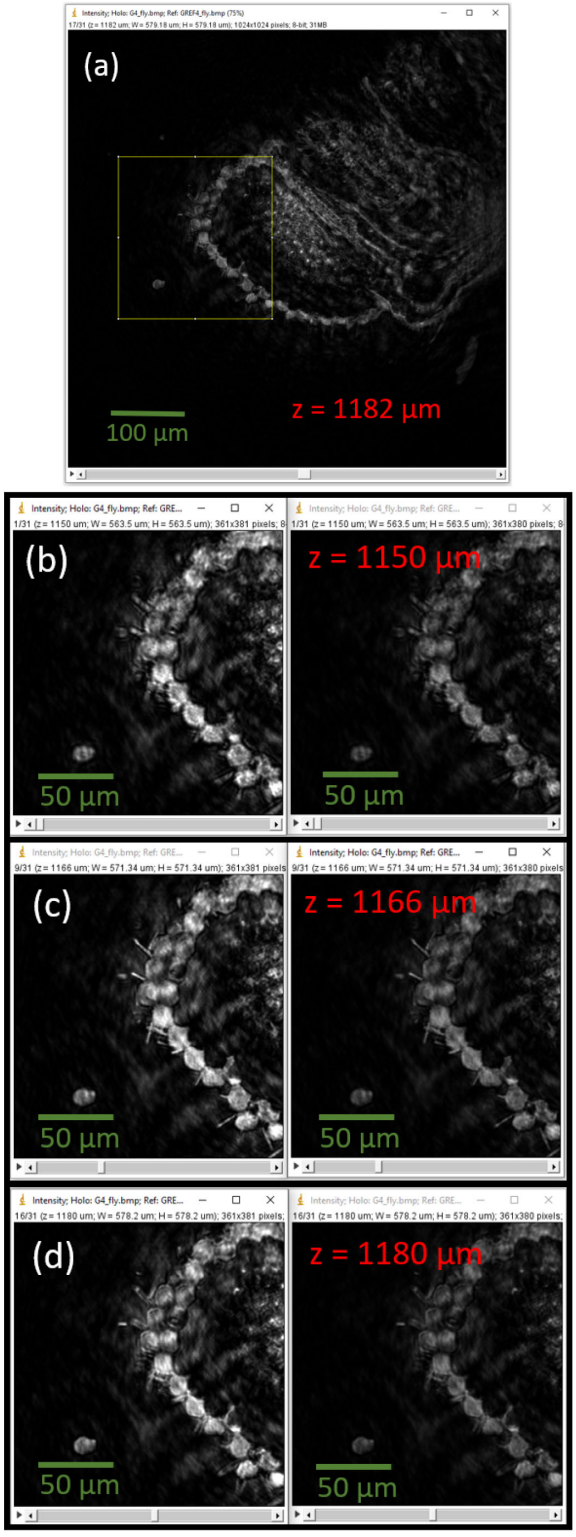

Fig. 10. DLHM reconstruction of an experimental hologram of the section of the head of a *drosophila melanogaster* fly. (a) Full field of view DLHM intensity reconstruction of the specimen. (b)–(d) Cropped intensity reconstructions from (a) for different source-to-sample distances with both the "enhanced contrast" function of ImageJ applied (left) or not applied (right).

To further demonstrate the advantages of using the developed plugin and the ImageJ built-in tools to facilitate focusing tasks in DLHM, an experimental hologram of the section of the head of the *drosophila melanogaster* fly has been selected. For this hologram, the manual determination of the focal plane is a challenging task considering the intricate structure of the specimen, as shown in Fig. 10.

This DLHM hologram has been recorded with a source-to-screen distance of 14 mm, a 532 nm wavelength laser, and CCD camera with a square sensor of width/height of 6.86 mm and 1024 × 1024 pixels. The specimen is expected to be in focus in a plane at a reconstruction distance within a range of source-to-sample distances between 1.1 and 1.2 mm. In Fig. 10 Panel (a), an intensity reconstruction of the specimen is shown. To simplify the focal plane determination, a batch reconstruction for this hologram has been launched. Over this stack of reconstructions, a zone enclosed by the yellow line square in Panel (a) has been cropped. Over this cropped stack of intensity reconstructions, the Enhanced Contrast function of ImageJ has been applied. Three planes of the cropped stack, reconstructed at 1150, 1166, and 1180 µm are presented in Fig. 10, Panels (b), (c), and (d), respectively. In each panel, both the output of the reconstruction module (right) and the contrast-enhanced image (left) are shown. As can be observed in Fig. 10, the determination of the focal plane for this experimental sample can be further simplified by using one of the built-in tools of ImageJ to improve the visualization of the reconstructions. The experimental DLHM holograms to obtain the intensity reconstructions presented in this section are all available via direct download in the Examples section in [27].

5. CONCLUSIONS

In this paper, an ImageJ open-source plugin for the numerical simulation and reconstruction of DLHM holograms has been presented. Two modules compose the presented plugin, simulation, and reconstruction.

In the simulation module, via a discrete implementation of the Rayleigh–Somerfield diffraction formula for numerical propagations, the user can easily create a simulated DLHM hologram from a known amplitude-phase distribution. This module only requires as inputs the parameters associated with the geometry of the simulated DLHM setup and 2D images that code the amplitude-phase distributions in gray levels. The simulation module outputs the simulated hologram, the reference hologram, and/or the contrast hologram. This module has been effectively used to validate the relationship between the lateral resolution of a DLHM setup with its numerical aperture.

In the reconstruction module, by means of a discrete implementation of a scalar diffraction integral, the numerical propagation for the reconstruction of DLHM holograms of experimental or simulated samples can be straightforwardly executed in a user-friendly interface. The reconstruction module reads the input hologram as a 2D image in either format and only requires the insertion of the parameters related to the acquisition or simulated setup and the desired source-to-sample distance. The batch reconstruction feature of this module also allows easy inspection of a given reconstruction volume by producing a movie-like batch of reconstructions. This module has been successfully validated on reconstructing and properly

focusing experimental DLHM holograms of different microorganisms in water and the section of the head of a *drosophila melanogaster* fly.

The computing of the numerical simulation and/or reconstruction of DLHM holograms within the robust environment of ImageJ greatly simplifies the analysis, enhancing, packing, and sorting (among other tasks) of the retrieved information. Furthermore, because our plugin allows us to create output images with physical dimensions and parameters—for instance, micrometers and phase rather than pixels and gray levels—the post-manipulation of the output images is significantly eased by using the built-in set of tools provided by ImageJ. The reader is referred to the plugin documentation and/or contact our group for further information.

Funding. Universidad Nacional de Colombia; Universidad EAFIT.

Acknowledgment. We thank the Optics Laboratory for the use of its equipment. C. Trujillo acknowledges the support by Vicerrectoría de Descubrimiento y Creación de la Universidad EAFIT.

Disclosures. The authors declare no conflicts of interest.

REFERENCES

1. D. Gabor, "A new microscopic principles," Nature **161**, 777–778 (1948).
2. J. Garcia-Sucerquia, W. Xu, S. K. Jericho, P. Klages, M. H. Jericho, and H. J. Kreuzer, "Digital in-line holographic microscopy," Appl. Opt. **45**, 836–850 (2006).
3. J. Garcia-Sucerquia, D. C. C. Alvarez-Palacio, and H. J. J. Kreuzer, "High resolution Talbot self-imaging applied to structural characterization of self-assembled monolayers of microspheres," Appl. Opt. **47**, 4723–4728 (2008).
4. M. Kanka, R. Riesenberg, P. Petruck, and C. Graulig, "High resolution (NA = 0.8) in lensless in-line holographic microscopy with glass sample carriers," Opt. Lett. **36**, 3651–3653 (2011).
5. S. K. Jericho, P. Klages, J. Nadeau, E. M. Dumas, M. H. Jericho, and H. J. Kreuzer, "In-line digital holographic microscopy for terrestrial and exobiological research," Planet. Space Sci. **58**, 701–705 (2010).
6. B. Patiño-Jurado, J. F. Botero-Cadavid, and J. Garcia-Sucerquia, "Cone-shaped optical fiber tip for cost-effective digital lensless holographic microscopy," Appl. Opt. **59**, 2969–2975 (2020).
7. W. Xu, M. H. Jericho, I. A. Meinertzhagen, and H. J. Kreuzer, "Digital in-line holography for biological applications," Proc. Natl. Acad. Sci. USA **98**, 11301–11305 (2001).
8. S. K. K. Jericho, J. Garcia-Sucerquia, W. Xu, M. H. H. Jericho, and H. J. J. Kreuzer, "Submersible digital in-line holographic microscope," Rev. Sci. Instrum. **77**, 43706–43710 (2006).
9. M. H. Jericho, H. J. Kreuzer, M. Kanka, and R. Riesenberg, "Quantitative phase and refractive index measurements with point-source digital in-line holographic microscopy," Appl. Opt. **51**, 1503–1515 (2012).
10. D. C. Alvarez-Palacio and J. Garcia-Sucerquia, "Lensless microscopy technique for static and dynamic colloidal systems," J. Colloid Interface Sci. **349**, 637–640 (2010).
11. D. A. Hincapie, C. Restrepo, H. Casanova, J. Kreuzer, and J. Garcia-Sucerquia, "Colloidal stability evaluation via digital in-line holographic microscopy," in *Digital Holography and Three-Dimensional Imaging*, OSA Technical Digest, 2008, paper DTuC7.
12. B. Patiño, J. Botero-Cadavid, and J. Garcia-Sucerquia, "Cone-shaped optical fiber tip for cost-effective digital lensless holographic microscopy," Appl. Opt. **59**, 2969–2975 (2020).
13. C. T. Rueden, J. Schindelin, M. C. Hiner, B. E. DeZonia, A. E. Walter, E. T. Arena, and K. W. Eliceiri, "ImageJ2: ImageJ for the next generation of scientific image data," BMC Bioinf. **18**, 529 (2017).
14. J. W. Goodman, *Introduction to Fourier Optics* (Robert & Company, 2005).
15. P. Hariharan, *Optical Holography: Principles, Techniques, and Applications*, 2nd ed. (Cambridge University, 1996).
16. J. F. Restrepo and J. Garcia-Sucerquia, "Magnified reconstruction of digitally recorded holograms by Fresnel-Bluestein transform," Appl. Opt. **49**, 6430–6435 (2010).
17. J. F. Restrepo and J. Garcia-Sucerquia, "Diffraction-based modeling of high-numerical-aperture in-line lensless holograms," Appl. Opt. **50**, 1745–1752 (2011).
18. C. Mann, L. Yu, C.-M. Lo, and M. Kim, "High-resolution quantitative phase-contrast microscopy by digital holography," Opt. Express **13**, 8693–8698 (2005).
19. T. Shimobaba, J. Weng, T. Sakurai, N. Okada, T. Nishitsuji, N. Takada, A. Shiraki, N. Masuda, and T. Ito, "Computational wave optics library for C++: CWO++ library," Comput. Phys. Commun. **183**, 1124–1138 (2012).
20. P. Piedrahita-Quintero, R. Castañeda, and J. Garcia-Sucerquia, "Numerical wave propagation in ImageJ," Appl. Opt. **54**, 6410–6415 (2015).
21. H. J. Kreuzer, "Holographic microscope and method of hologram reconstruction," U.S. patent 6,411,406 B1 (25 June 2002).
22. M. Frigo and S. G. Johnson, "FFTW: an adaptive software architecture for the FFT," in *IEEE International Conference on Acoustics, Speech and Signal Processing* (1998), Vol. **3**, pp. 1381–1384.
23. P. Piedrahita-Quintero, C. Trujillo, and J. Garcia-Sucerquia, "JDiffraction: a GPGPU-accelerated JAVA library for numerical propagation of scalar wave fields," Comput. Phys. Commun. **214**, 128–139 (2017).
24. M. H. Jericho and H. J. Kreuzer, "Point source digital in-line holographic microscopy," in *Coherent Light Microscopy*, P. Ferraro, A. Wax, and Z. Zalevvsky, eds. (Springer, 2011), pp. 3–30.
25. J. Garcia-Sucerquia, C. Trujillo, and J. Restrepo Agudelo, "Microscopio holográfico digital sin lentes (MHDSL) y método para visualizar muestras," U.S. patent 1425894300 (31 May 2016).
26. "ImageJ download and install," https://imagej.nih.gov/ij/download.html.
27. J. P. Piedrahita, C. Trujillo, and J. García-Sucerquia, "Digital lensless holographic microscopy," https://unal-optodigital.github.io/DLHM/.
28. P. Wendykier, "JTransforms," https://sites.google.com/site/piotrwendykier/software/jtransforms.
29. R. Castañeda, J. Piedrahita, and J. García-Sucerquia, "Numerical propagation plugin for ImageJ," https://unal-optodigital.github.io/NumericalPropagation/.
30. F. Abrantes and I. M. Gil, "Marine diatoms," in *Encyclopedia of Quaternary Science*, 2nd ed. (2013).
31. T. Asakura, "Resolution of two unequally bright points with partially coherent light," Nouv. Rev. Opt. **5**, 169–177 (1974).